Barrier effect of grain boundaries on the avalanche propagation of polycrystalline plasticity

Tomoaki Niiyama and Tomotsugu Shimokawa

Barrier effect of grain boundaries on the avalanche propagation of polycrystalline plasticity

Tomoaki Niiyama* and Tomotsugu Shimokawa
College of Science and Engineering, Kanazawa University,
Kakuma-machi, Kanazawa, Ishikawa 920-1192, Japan and
Faculty of Mechanical Engineering, Kanazawa University,
Kakuma-machi, Kanazawa, Ishikawa 920-1192, Japan
(Dated: August 19, 2016)

To investigate the barrier effect of grain boundaries on the propagation of avalanche-like plasticity at the atomic-scale, we perform three-dimensional molecular dynamics simulations by using simplified polycrystal models including symmetric-tilt grain boundaries. The cut-offs of stress-drop distributions following power-law distributions decrease as the size of the crystal grains decreases. We show that some deformation avalanches are confined by grain boundaries; on the other hand, unignorable avalanches penetrate all the grain boundaries included in the models. The blocking probability that one grain boundary hinders this system-spanning avalanche is evaluated by using an elemental probabilistic model.

A new insight into crystalline plasticity has been provided from non-equilibrium physics at the beginning of the century. Discontinuous, stick-slip plastic deformation, referred to as *intermittent plasticity*, has been revealed as an intrinsic nature of plasticity in crystalline solids[1–8]; the probability of a deformation event with a magnitude s follows a *power-law distribution*, $P(s) \propto s^{-\beta}$, where β is a constant. This power-law distribution is a fingerprint of the presence of non-equilibrium critical phenomena especially self-organized criticality[9,10].

A combination of acoustic emission measurements and numerical simulations using discrete-dislocation dynamics have revealed that the power-law behavior of plasticity is caused by *avalanches* of dislocation motions[2,6]. The acoustic emission measurements in the creep of polycrystal ices have indicated that *grain boundaries (GBs)*, i.e., interfaces between crystal grains, can act as obstacles to the avalanches[11,12]. Louchet *et al.* have introduced a new concept regarding the plastic deformation of polycrystals, which is one of the most fundamental subjects in material science; polycrystal yielding occurs when the avalanche transmits across GBs and percolates through the material[13]. Thus, the elucidation of the interaction between GBs and avalanches of plasticity would advance our understanding regarding the features of plastic deformation of polycrystals, in particular, the grain size dependence of plastic yielding[14–16].

The interaction between single dislocations and GBs has been extensively investigated[17–19], but the quantification of the interaction between avalanches of dislocations is still quite preliminary. The consequence of the avalanche statistics by GBs has been discussed through discrete-dislocation dynamics[20]. However, the dislocation-GB interaction is truly atomic-scale dynamics. Therefore, molecular dynamics (MD) simulations for this issue are desperately needed to provide a correct description and quantification of the interaction. Recently, intermittent plasticity in single crystals has been successfully reproduced by MD simulations[21,22]. However, intermittent plasticity in polycrystals remains unaddressed.

In this study, by performing MD simulations with polycrystal models consisting of some symmetric-tilt GBs, we prove and evaluate the role of GBs as obstacles for intermittent plasticity. In particular, we demonstrate the statistical distribution of the mechanical response of tensile deformation, its dependence on the grain size, and the atomic-scale dynamics of avalanche motion in the polycrystal models. Finally, we attempt to quantify the blocking probability of avalanche propagation by GBs.

We performed three-dimensional MD simulations of uniaxial tensile deformation of aluminum polycrystals under constant temperature and strain rate condition with different grain sizes, by applying the embedded atom potential presented by Mishin *et al.* to the atomic interaction[23]. For the simulations, we employed polycrystal models simplified as lamellar stacking structures containing several $\langle 112 \rangle \Sigma 11$ symmetric-tilt GBs, which align normal to the tensile direction. Owing to this alignment, GB sliding and grain-growth are sufficiently suppressed in this simulation because neither process contributes to releasing the tensile stress. There are various types of GBs, such as symmetric, asymmetric, and twisted[24]; for simplicity, we employed symmetric-tilt GBs for initial the trials.

Here we describe the procedure for preparing the polycrystal models including $\langle 112 \rangle \Sigma 11$ symmetric-tilt GBs. First, let us consider two fcc lattices, whose $[11\bar{1}]$, $[112]$, and $[1\bar{1}0]$ axes are along the x, y, and z directions, respectively. Next, we tilt the fcc lattices around the $[112]$ axis by $+\theta/2$ and $-\theta/2$, respectively. The GB misorientation angle $\theta/2 = \tan^{-1} \sqrt{3/8} \simeq 31.48°$ is chosen. GBs with this angle are called $\Sigma 11$ GBs[24,25]. If one joins those lattices at an xy-plane interface, the interface is the $\langle 112 \rangle \Sigma 11$ symmetric-tilt GB. Both tilted lattices with the lattice constant of aluminum a_0 have a unit cell with minimum periodic lengths along x, y, and z; $\Delta L_x = \sqrt{33/2}a_0$, $\Delta L_y = \sqrt{3/2}a_0$, and $\Delta L_z = \sqrt{11}a_0$. Thus, one can apply the periodic boundary conditions to the lattices without destructing the translational symmetry, in so far as the lengths of a simulation cell along the three directions are equal to the integral multiple of the corresponding minimum periodic length of the tilted lattices. For the present simulations, we chose the dimensions of the simulation cell: $L_x = 8\Delta L_x \simeq 13.2$ nm, $L_y = 24\Delta L_y \simeq 11.9$ nm, and $L_z = 12\Delta L_z \simeq 16.2$ nm, where the cell is filled with 152064 atoms. Periodic boundary conditions were applied to the simulation cell. In this dimension, if the three unit cells with $+\theta/2$ are alternately stacked with three unit cells with $-\theta/2$ along the z-axis in layers, a lamellar stacked polycrystal model is obtained with four GBs as
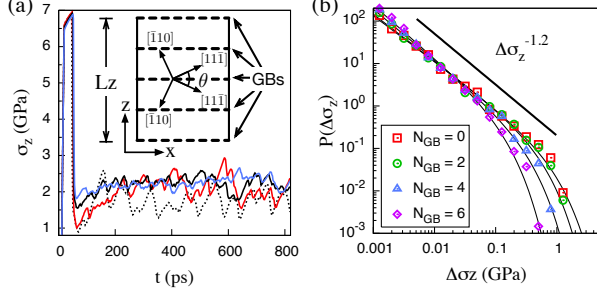
FIG. 1. (a) Typical stress-time curves, where the tensile stress $\sigma_z(t)$ of N_{GB} = 0, 2, 4, and 6 models are depicted as dashed black, solid red, black, and blue lines, respectively. The schematic figure of the polycrystal models used in this study is imposed. (b) The probability distributions of stress drop, $\Delta\sigma_z$, in each model, where the empirical distributions in Eq. (2) fitted to each distribution are shown as thin black curves.

TABLE I. The values of the power-law exponent β, the cut-offs $\Delta\sigma_c$, and the frequency of occurrence of system-spanning deformation events n_{SS} and all deformation events n_{def}.

N_{GB}	β	$\Delta\sigma_c$ (GPa)	n_{SS}	n_{def}
0	1.11	0.788	142	644
2	1.08	0.480	123	694
4	1.19	0.288	126	870
6	1.24	0.121	126	1080

depicted in Fig. 1(a). Following, we prepared four models with 0, 2, 4, and 6 GBs by employing the layer thickness corresponding to the grain sizes $12\Delta L_z$, $6\Delta L_z$, $3\Delta L_z$, and $2\Delta L_z$, respectively. We distinguish these models by the number of GBs, N_{GB}.

Using the polycrystal models as initial configurations and random numbers as initial velocities for all atoms, we performed MD simulations for uniaxial tensile deformation along the z-axis until 50 % deformation is attained. During the simulations, the pressures along the x- and y-axes were maintained zero using the Parrinello-Rahman method without shear[26]. To save computing time for the simulations, we applied a strain rate 10^{10} s^{-1} at the early stage of the deformation to 10 % when the deformation is purely elastic. After that, the strain rate was changed to 5×10^8 s^{-1}. For each model, we performed the MD simulations 20 times with different initial velocities for all atoms.

For the simulations, we used Langevin's dynamics represented by the equation of atom motion[27];

$$m_i\ddot{\boldsymbol{q}}_i(t) = \boldsymbol{F}_i - m_i\gamma\dot{\boldsymbol{q}}_i(t) + \sqrt{2m_i\gamma k_B T}\,\boldsymbol{\eta}_i(t), \qquad (1)$$

where m_i is the mass of the i-th atom, $\boldsymbol{q}_i$ and $\boldsymbol{F}_i$ are the position and the force vector of the i-th atom, respectively. k_B, T, γ, and $\boldsymbol{\eta}_i(t)$ are Boltzmann's constant, temperature, the friction coefficient, and the random force vector as a white noise, respectively. In the present study, we chose γ = 1 ps^{-1}. The selected temperature was 10 K, to reduce thermal fluctuations[22]. This equation of motion is also employed to the dynamics of the simulation cell. The second-order accurate algorithm developed by Vanden-Eijinden and Ciccotti was used for the numerical integration of the dynamics[27,28]. To generate the random forces, Mersenne Twister generator was employed[29].

The noise-induced dynamics not only keeps the temperature constant but also depresses stress fluctuations irrelevant to plastic deformation; the fluctuations are caused by phonon propagation or periodic dislocation motion such as string vibration after large-scale plastic deformation events.

The tensile stress of all the models, $\sigma_z(t)$, obtained from

the simulation results shows intermittent plastic manners as depicted in Fig. 1(a); $\sigma_z(t)$ gradually increases by elastic deformation and abruptly drops by repeated plastic deformation, where the time-series are averaged over a 0.2 ps interval to remove thermal fluctuations. This serrated behavior is the same as the intermittent plasticity observed in previous numerical studies[21,22], but the amplitude of the stress fluctuation decreases as N_{GB} increases.

The stress-drop distribution extracted from the average time-series are shown in Fig. 1(b). The value of stress drop, $\Delta\sigma_z$, is defined as the reduction amount of σ_z during *a plastic deformation event* from t_{start} to t_{end}; $\Delta\sigma_z = \sigma_z(t_{start}) - \sigma_z(t_{end})$. Plastic deformation events can be determined as periods during which $\sigma_z(t)$ monotonically decreases as explained in the previous study[22]. In the figure, all the distributions indicate algebraic decay in the range of $\Delta\sigma_z < 0.1$ GPa. This feature corresponds to a power-law behavior, which is consistent with the results obtained in previous numerical studies employing MD[21,22] and discrete-dislocation dynamics simulations[2,6,7], but there is a notable difference. That is, the distributions have different *cut-offs*, which are rapid decreases of probability at a large-scale regime. We evaluated the cut-offs of the distributions by fitting the following empirical relationship to each distribution:

$$P(\Delta\sigma_z) \approx \Delta\sigma_z^{-\beta}\exp(-\Delta\sigma_z/\Delta\sigma_c), \qquad (2)$$

where β and $\Delta\sigma_c$ are the power-law exponent and the characteristic scale of stress drops, respectively. The values of β and $\Delta\sigma_c$ obtained by the fitting are listed in Table I. As can be seen from the table and Fig. 1(b), $\Delta\sigma_c$ decreases as the number of GBs in each model increases, whereas the exponents of the models are almost the same ($\beta \simeq 1.2$). This trend of the cut-offs supports that our MD simulations reproduce the role of GBs as obstacles to the avalanches consistent with the previous experimental study[11].

In addition to the role of GBs revealed from the macroscopic responses, MD simulations can allow us to confirm this behavior directly by observing microscopic-scale dynamics during the deformation process. Here we analyze statistically the linear size of a slip area, during a plastic deformation event, by identifying slip areas in the following way.

Let us consider the set of 12 nearest neighbor atoms around the i-th atom at time t. We denote these atoms by $\boldsymbol{n}^{(i)}(t) = \{n_1, n_2, ..., n_{12}\}$, where $n_1^{(i)}, n_2^{(i)}, ..., n_{12}^{(i)}$ are integers which identify the neighbor atoms around the i-th atom. If the set of the atoms at t_{start} is different from that at t_{end}, i.e., $\boldsymbol{n}^{(i)}(t_{start}) \neq$
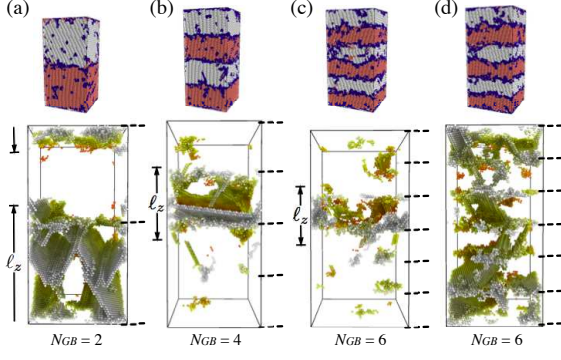
FIG. 2. Snapshots of all atoms (top) and participant atoms representing slip areas during a plastic deformation event (bottom) in (a) the model with $N_{GB} = 2$, (b) $N_{GB} = 4$, (c, d) $N_{GB} = 6$. The approximate positions of GBs are indicated by horizontal dashed lines. (d) The slip area percolates all the GBs in the model.
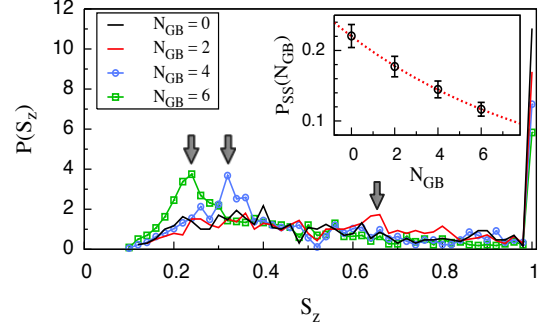
FIG. 3. The distributions of the relative linear size of an avalanche S_z. The inset shows the probability of system-spanning events plotted against the number of GBs, N_{GB}. Open circles and the red dotted line indicate the probability estimated from the simulation results in Table I and the theoretical relationship depicted in Eq.(3), respectively.

$\boldsymbol{n}^{(i)}(t_{end})$, the i-th atom is regarded as a participant atom to the deformation event starting at t_{start}. Applying this procedure to all the atoms at a deformation event one can identify the participant atoms that represent the slip area caused by the deformation event. By following this procedure, we extract all the participant atoms from the numerical results that are averaged with 1 ps intervals.

Typical configurations of participant atoms identified by the above procedure are depicted in the bottom panels of Fig. 2, where smaller clusters consisting of less than 12 participant atoms are removed for the visibility. The participant atoms formed into sheets as shown in the panels follow the trail of dislocations. From the bottom panels of Figs. 2(a), (b), and (c), it can be directly confirmed that GBs confine the propagation of an avalanche. However, not all avalanches are blocked by GBs. For instance, Fig.2(d) shows *a system-spanning deformation event* in which a slip area penetrates all the GBs in the system, even the system contains six GBs. Thus, the statistics of the spatial extension of the avalanches should be investigated quantitatively.

Note that we confirm neither fracture nor crack nucleation in the simulations owing to the high ductility of aluminum. For instance, the upper panels of Fig. 2 show snapshots of all the atoms at the same moments as in the bottom panels, where atoms with a defect-type lattice structure are colored blue, and fcc structure atoms are colored red and gray in accordance with their orientation angles. The snapshots clearly indicate neither cracks nor fracture.

Here we evaluate the linear size of one avalanche along the z-axis by the following. The cluster analysis is performed to participant atoms during a deformation event; participant atoms whose distance between each other is $< 1.2a_0/\sqrt{2}$ are regarded as a member of one common cluster consisting of an isolated slip area. The length along the z-axis of the largest one of all the clusters during the event is denoted by ℓ_z. We represent the relative propagation length of an avalanche as $S_z \equiv \ell_z/L_z$. For instance, S_z will be $1/N_{GB}$ in the model con-

taining N_{GB} GBs when an avalanche emerging from a crystal grain is completely blocked by the neighboring GBs. On the other hand, if an avalanche percolates through the system, one can obtain $S_z = 1$.

The statistical distributions $P(S_z)$ calculated from all the configurations of participant atoms are shown in Fig. 3. One can find typical peaks (indicated by arrows) at $S_z = 0.67, 0.33$, and 0.25 for $N_{GB} = 2$, 4, and 6, respectively, even though the peak at $S_z = 0.67$ is vague. These are only slightly larger than the corresponding characteristic lengths of a crystal grain in each model, $1/N_{GB}$. This agreement clearly indicates an effect of GBs to block the propagation of avalanches of plasticity. The fact that there are no typical peaks in the model with $N_{GB} = 0$ also supports the presence of the effect indirectly. In contrast to the typical peaks providing evidence of the barrier effect, all the distributions have significant peaks at $S_z = 1$, which corresponds to system-spanning deformation events as depicted in Fig. 2(d), for instance. These significant peaks mean that not a few avalanches pass through all GBs. Because the linear size of such a system-spanning avalanche event cannot be defined, evaluating the mean free-path of the avalanches is impossible. Thus, it is also impossible to quantify the barrier effect of GBs by assessing the mean free-path.

To overcome this difficulty, we focus on the system-spanning events rather than on all the deformation events. We now evaluate *the blocking probability*; the probability that one GB hinders a system-spanning avalanche. In other words, the probability that a deformation event evolves to a system-spanning event is considered. This probability can be estimated by the relative frequency of the system-spanning events; $P_{SS}(N_{GB}) = n_{SS}/n_{def}$, where n_{SS} and n_{def} are the frequency of the system-spanning avalanche events and that of all deformation events, respectively. In Table I, we enumerate n_{SS} and n_{def} obtained from the present simulations. The inset in Fig. 3 shows the system-spanning probability estimated from the data plotted by open circles as a function of N_{GB}, where the error bars are approximately calculated from a

standard deviation of the binomial distribution with the number of trials n_{def} and the probability in each trial n_{SS}/n_{def}.

The estimated probability in Fig. 3 monotonically decreases with the increase of N_{GB}. In other words, the propagation of an avalanche of plasticity is quickly damped as the grain size (grain thickness) is small. Thus, the present result is direct evidence of the barrier effect of GBs upon the avalanche propagation.

If one GB decreases P_{SS} independently by the factor α ($\leq$ 1), the probability in the model including N_{GB} GBs can be described by the simple relationship:

$$P_{SS}(N_{GB}) = P_{SS}(0)\,\alpha^{N_{GB}}, \qquad (3)$$

where $1-\alpha$ corresponds to the blocking probability of system-spanning avalanches by one GB. This theoretical relationship can fit well with the estimated probability by the least squares method with the parameters $P_{SS}(0) = 0.22$ and $\alpha = 0.90$ as shown in Fig. 3(c).

The theoretical relationship of Eq. (3) is made on the basis of two assumptions; (i) the emergence of the avalanches is independent of the presence of GBs, and (ii) a GB blocks a system-spanning avalanche independently with the blocking probability $1 - \alpha$. While these assumptions might be disputable, there is collateral evidence of the former assumption. That is, the power-law exponent of the stress-drop distribution β does not depend on N_{GB} as shown in Fig. 1(b) and Table I. This trend implies that avalanches occur in the same fashion inside grains. The excellent agreement between the theoretical curve and the estimated probability (the inset in Fig. 3) supports the assumption (ii). Hence, we can conclude that this fitting can provide us with an estimated value of the barrier capability of the GB against the avalanche of crystalline plasticity.

An unchanged of β is inconsistent with the previous experimental observations[11], whereas the change of $\Delta\sigma_c$ is consistent with them. This inconsistency might be because of the simplification of the present polycrystal models. That is, the present result intimates that modulation of β observed in the previous experiment[11] results from complicated domain structures, variation in the size of grains, or both as is common in real polycrystals. This complexity might produce some slow relaxation processes such as GB sliding or grain-growth, which can affect the avalanche properties[31,32]. The presence of surface might also be important for the avalanche dynamics[33,34]. MD simulations employing such realistic poly-crystal models are required to prove the cause of the modulation.

To evaluate the barrier effect of a particular kind of GBs, simplified polycrystal models similar to those used in this study is appropriate rather than realistic polycrystal models. It is expected that the factor α depends on the misorientation angle of the tilt-and-twist GBs. Investigation of the barrier effect of these GBs is an issue for future studies.

The quantification of the barrier effect in this study will contribute to the construction of theoretical models or semi-macroscopic numerical models, such as models for the discrete-dislocation dynamics or the phase field method for polycrystalline solids, which worked well for the investigation of the avalanche behaviors in single crystals[2,6,30]. These models will shed light on the mechanical properties of poly-crystalline materials from the viewpoint of intermittent plasticity.

In this study, to investigate the interaction between the avalanche-like propagation of plasticity and the grain boundaries (GBs) in polycrystalline solids at the atomic-scale, we performed molecular dynamics simulations for uniaxial tensile deformation in aluminum polycrystal models simplified as lamellar stacking structure including symmetric-tilt GBs. The results show that the stress drops caused by an avalanche of plastic deformation follow power-law distributions even in polycrystals, but the cut-off of the distribution decreases with decreasing grain size. By observing atomic-scale dynamics of the simulation results, we noted that some avalanches are confined by GBs, but others transmit across the GBs or penetrate through the system entirely (system-spanning avalanches). We propose the theoretical description of the system-spanning probability in the models. The excellent agreement between the theoretical probability and the estimated probability from the simulations provides us with the blocking probability of the avalanches by single-grain boundary.

[*] niyama@se.kanazawa-u.ac.jp

[1] G. Ananthakrishna, S. J. Noronha, C. Fressengeas, and L. P. Kubin, *Crossover from chaotic to self-organized critical dynamics in jerky flow of single crystals*, Phys. Rev. E **60**, 5455 (1999).

[2] M. C. Miguel, A. Vespignani, S. Zapperi, J. Weiss, and J.-R. Grasso, *Intermittent dislocation flow in viscoplastic deformation*, Nature **410**, 667 (2001).

[3] M. Zaiser, *Scale invariance in plastic flow of crystalline solids*, Advances in Physics **55**, 185 (2006).

[4] G. Ananthakrishna, *Current theoretical approaches to collective behavior of dislocations*, Physics Reports **440**, 113 (2007).

[5] J. P. Sethna, *Crackling wires*, Science **318**, 207 (2007).

[6] F. F. Csikor, C. Motz, D. Weygand, M. Zaiser, and S. Zapperi, *Dislocation avalanches, strain bursts, and the problem of plastic forming at the micrometer scale*, Science **318**, 251 (2007).

[7] G. Tsekenis, J. T. Uhl, N. Goldenfeld, and K. A. Dahmen, EPL (Europhysics Letters) *Determination of the universality class of crystal plasticity*, **101**, 36003 (2013).

[8] J. Weiss, T. Richeton, F. Louchet, F. Chmelik, P. Dobron, D. Entemeyer, M. Lebyodkin, T. Lebedkina, C. Fressengeas, and R. J. McDonald, *Evidence for universal intermittent crystal plasticity from acoustic emission and high-resolution extensometry experiments*, Phys. Rev. B **76**, 224110 (2007).

[9] P. Bak, C. Tang, and K. Wiesenfeld, *Self-organized criticality: An explanation of the 1/f noise*, Phys. Rev. Lett. **59**, 381 (1987).

[10] H. J. Jensen, *Self-Organized Criticality: Emergent Complex Behavior in Physical and Biological Systems (Cambridge Lecture Notes in Physics)* (Cambridge University Press, 1998).

[11] T. Richeton, J. Weiss, and F. Louchet, *Breakdown of avalanche critical behaviour in polycrystalline plasticity*, Nat Mater **4**, 465 (2005).

[12] T. Richeton, J. Weiss, and F. Louchet, *Dislocation avalanches: Role of temperature, grain size and strain hardening*, Acta Materialia **53**, 4463 (2005).

[13] F. Louchet, J. Weiss, and T. Richeton, *Hall-petch law revisited in terms of collective dislocation dynamics*, Phys. Rev. Lett. **97**, 075504 (2006).

[14] E. O. Hall, *The deformation and ageing of mild steel: Iii discussion of results*, Proceedings of the Physical Society. Section B **64**, 747 (1951).

[15] N. J. Petch, *The cleavage strength of polycrystals*, J. Iron Steel Inst. **174**, 25 (1953).

[16] M. Meyers, A. Mishra, and D. Benson, *Mechanical properties of nanocrystalline materials*, Progress in Materials Science **51**, 427 (2006).

[17] J. Livingston and B. Chalmers, *Multiple slip in bicrystal deformation*, Acta Metallurgica **5**, 322 (1957).

[18] Z. Shen, R. Wagoner, and W. Clark, *Dislocation and grain boundary interactions in metals*, Acta Metallurgica **36**, 3231 (1988).

[19] Y. Shibutani, T. Hirouchi, and T. Tsuru, *Transfer and incorporation of dislocations to Σ3 tilt grain boundaries under uniaxial compression*, Journal of Solid Mechanics and Materials Engineering **7**, 571 (2013).

[20] P. Moretti, L. Laurson, and M. J. Alava, *Dislocation interactions mediated by grain boundaries*, Journal of Statistical Mechanics: Theory and Experiment **2008**, P05010 (2008).

[21] P. Moretti, B. Cerruti, and M.-C. Miguel, *Yielding and irreversible deformation below the microscale: Surface effects and non-mean-field plastic avalanches*, PloS one **6**, e20418 (2011).

[22] T. Niiyama and T. Shimokawa, *Atomistic mechanisms of intermittent plasticity in metals: Dislocation avalanches and defect cluster pinning*, Phys. Rev. E **91**, 022401 (2015).

[23] Y. Mishin, D. Farkas, M. J. Mehl, and D. A. Papaconstantopoulos, *Interatomic potentials for monoatomic metals from experimental data and ab initio calculations*, Phys. Rev. B **59**, 3393 (1999).

[24] A. Sutton and R. Balluffi, *Interfaces in crystalline materials* (Clarendon Press, 1995).

[25] T. Shimokawa, *Asymmetric ability of grain boundaries to generate dislocations under tensile or compressive loadings*, Phys. Rev. B **82**, 174122 (2010).

[26] M. Parrinello and A. Rahman, *Crystal structure and pair potentials: A molecular-dynamics study*, Phys. Rev. Lett. **45**, 1196 (1980).

[27] M. Tuckerman, *Statistical mechanics: theory and molecular simulation* (Oxford Graduate Texts, 2010).

[28] E. Vanden-Eijnden and G. Ciccotti, *Second-order integrators for langevin equations with holonomic constraints*, Chemical Physics Letters **429**, 310 (2006).

[29] M. Matsumoto and T. Nishimura, *Mersenne twister: A 623-dimensionally equidistributed uniform pseudo-random number generator*, ACM Trans. Model. Comput. Simul. **8**, 3 (1998).

[30] M. Koslowski, R. LeSar, and R. Thomson, *Avalanches and scaling in plastic deformation*, Phys. Rev. Lett. **93**, 125502 (2004).

[31] S. Papanikolaou, D. M. Dimiduk, W. Choi, J. P. Sethna, M. D. Uchic, C. F. Woodward, and S. Zapperi, *Quasi-periodic events in crystal plasticity and the self-organized avalanche oscillator*, Nature **490**, 517 (2012).

[32] J. W. Cahn, Y. Mishin, and A. Suzuki, *Coupling grain boundary motion to shear deformation*, Acta Materialia **54**, 4953 (2006).

[33] G. Po, M. S. Mohamed, T. Crosby, C. Erel, A. El-Azab, and N. Ghoniem, *Recent Progress in Discrete Dislocation Dynamics and Its Applications to Micro Plasticity*, JOM **66**, 2108 (2014).

[34] S. Papanikolaou, H. Song, and E. Van der Giessen, *Obstacles and sources in dislocation dynamics: Strengthening and statistics of abrupt plastic events in nanopillar compression*, arXiv: 1511.04613 (2015).